During the period 1989-92 measured daily mean salinity ranged from 2.2 to 11.4 ppt in the Pamlico River and from 1 to 12.9 ppt in the Neuse River. Measured vertical salinity gradients in the upstream half of the Neuse River estuary were somewhat stronger than in the upstream half of the Pamlico River, but top-to-bottom differences in salinity in the lower half of the Neuse River estuary were generally 1.5 ppt or less. Higher salinities were observed on the north side of the Pamlico River estuary with a lateral difference of as much as 5 ppt during November, whereas higher salinities were generally on the south side of the Neuse River estuary.

Simulated circulation and transport for June 14 -24, 1991, indicate a greater range in transport in the Neuse River estuary than in the Pamlico. Cumulative transport over the simulation period was also greater in the Neuse. Similarly, particle tracks showed net movement of less than 8 km at each of 4 sites in the Pamlico and Neuse Rivers with the Neuse River showing somewhat greater total movement than in the Pamlico. Simulated currents were generally higher in the Neuse River than in the Pamlico River, where boundary water levels were out of phase as compared to the Neuse River where boundary water levels were in phase.

REFERENCES

Giese, G.L., Wilder, H.B., and Parker, G.G., 1985, Hydrology of major estuaries and sounds of North Carolina: U.S. Geological Survey Water-Supply Paper 2221, 108 p.

Leendertse, J.J., 1987, Aspects of SIMSYS2D, a system for two-dimensional flow computation: Santa Monica, California, RAND Corporation, Report No. R-3572-USGS, 80 p.

Pietrafesa, L.J., Janowitz, G.S., Chao, T.-Y., Wiesberg, R.H., Askari, F., and Noble, E., 1986, The physical oceanography of Pamlico Sound: Raleigh, University of North Carolina Sea Grant College Program, North Carolina State University, Working Paper 86-5, 125 p.

Schwartz, F.J., and Chestnut, A.F., 1973, Hydrographic atlas of North Carolina estuarine and sound waters, 1972: Raleigh, University of North Carolina Sea Grant College Program, North Carolina State University, Report No. UNC-SG-73-12, 132 p.

Signell, R.P., and Butnam, B., 1992, Modeling tidal exchange and dispersion in Boston Harbor: Journal of Geophysical Research, v. 97, no. C10, p. 15591-15606.

Westerink, J.J., and Gray, W.G., 1991, Progress in surface water modeling, *in* Reviews of Geophysics; U.S. National Report to International Union of Geodesy and Geophysics, p. 210-217.

Williams, A.B., Posner, G.S., Woods, W.J., and Duebler, E.E., 1967, A hydrographic atlas of larger North Carolina sounds: Morehead City, Institute of Marine Sciences, University of North Carolina, Report No. UNC-SG-73-02,129 p.

A Numerical Study of Hydraulic Jump and Mixing in a Stratified Channel With a Sill

Ping Chen[1,2], R. Grant Ingram[1] and Jianping Gan[1]

ABSTRACT

An x–z plane two dimensional primitive equation model is used to study sill effects in a narrow channel. The aim is to examine the generation of internal bores/waves, hydraulic jumps and associated mixing processes in continuously stratified water under tidal forcing. Different cases with various sill heights, tidal currents and stratifications are considered.

Results of these cases show complicated vertical structure of velocity and salinity, which differ from layer models but are similar to some observations. For selected cases of interest, supercritical conditions are reached at around maximum tidal current (both flooding and ebbing) in the sill region. Hydraulic jumps form at the location of the transition point from supercritical to subcritical, which is at lee side of sill and is consistent with layer theory in terms of composite Froude numbers. Internal bores will form at the jump location, propagate upstream across the sill and evolve into solitons when the current slackens. High turbulent kinetic energy, and strong mixing, occur not only in the jump but also in an extended area further downstream, where strong horizontal velocity shear and vertical velocity exist as a result of the jump. It is also found that unstable points occur in the upstream portion of the jump.

1. INTRODUCTION

Internal hydraulic controls and jumps in straits, narrow sounds and inlets have been commonly observed, i.e. in Knight Inlet (Farmer and Smith, 1980) and Manitounuk Sound (Gan and Ingram, 1992). When suitable subcritical flow passes a sill and/or a constriction, high velocity can be generated and the flow reaches supercritical condition. The flow is subject to two controls, one at upstream, where the flow changes from subcritical to supercritical, and another one downstream, where the flow changes from supercritical to subcritical. The downstream transition location, or control, usually exhibits an internal hydraulic

[1]Dept. of Atmos. and Oceanic Sci., McGill Univ., Montreal, PQ H3A 2K6
[2]Now at Program in Atmos. and Oceanic Sci., Princeton Univ., Princeton, NJ 08544

jump and strong mixing phenomena, and subsequently results in the propagation of internal waves and bores. The process may repeat if the forcing is periodic, such as tides.

The hydraulic controls of sill and constriction are traditionally studied with quasi-steady, layer models (i.e. Farmer and Denton, 1985 and Armi and Farmer, 1986). Such models are usually based on the Bernoulli equation applied for each layer and provide considerable insight into the dynamics of stratified flows through straits and over sills, where there is a distinct layer structure in the vertical. They are particularly useful for the study of controls. Lawrence (1985) gave detailed discussions on layer theory and predicted the crest control and approach control, which compared well to his laboratory experiment on flow past an obstacle. However, layer model cannot describe the jumps, although it can predict the location of a jump. This occurs because the layer models allow energy exchange between layers, while using energy conservation for the water column in spite of the high dissipation of energy in the jump region.

The internal bore propagation and its evolution into solitons has been successfully explained with the nonlinear Korteweg-de Vries (KdV) equation. However, there is a missing link between the internal hydraulic jump and the generation of a large amplitude internal bore for existing theory. In our study, we attempt to describe the jump, internal bore/soliton generation and propagation in an integrated approach using a numerical model.

We first consider that time dependency is important and should be included. In the aforementioned observations, tides were the primary driving force and internal waves and bores are pronounced unsteady phenomena associated with the tide-topography interaction and jumps. Farmer and Smith (1980) indicated that the time dependence of the tidal forcing is essential to the generation of the internal disturbances observed near the sill in Knight Inlet. The propagation of a bore in Manitounuk Sound was also examined by Gan and Ingram (1992). Geyer (1990) used a time-dependent, two layer model to study the flow over a sill. He indicated that the quasi-steady approximation is valid in the vicinity of the sill for the portion of the tidal cycle when the flow is transcritical, but the time-dependent term in the momentum equation becomes significant during the subcritical portion of the tidal cycle.

We next consider the inclusion of continuously stratified flow and vertical mixing. Layer flow theory assumes that the density is constant in each layer and disallows vertical mixing. Observations sometimes show high velocities in the middle of mixed water associated with a jump and no layer structure can be seen (e.g. Farmer and Denton, 1985). In Lawrence's laboratory experiment, he also observed a much distorted downstream velocity and density structure, while the two-layer form was maintained upstream. Gan and Ingram (1992) showed that inclusion of the pycnocline was important in the discussion of highly nonlinear processes.

Recently, Matsuura and Hibiya (1990) and Hibiya (1988) studied tidal flow-topography interaction using both experimental and numerical models. Their focus was the generation mechanism of the internal waves. The numerical model was two dimensional in the vertical plane and could accommodate non-hydrostatic and continuously stratified flow. They applied the model for a uniform statification (constant Brunt-Väisälä frequency N) with a constant vertical diffusivity. If one is to study a highly stratified water column it is preferable to use a computed, more realistic diffusivity, because of the complicated interaction between the high density gradient, which yields low diffusivity and tends to maintain the stratification, and the jump, which tends to breakup the stratification with high diffusivity.

In this study, our aim is to model the hydraulics of the tide-topography interaction, focussing on jumps and mixing, in a continuously stratified water column with time dependent barotropic tidal forcing and a turbulence closure scheme.

2. THE MODEL

2.1. Governing Equations

We consider the problem in the vertically two dimensional x–z plane (Figure 1), assuming the lateral variations of flow in narrow channel (y direction) are small and can be ignored. Under the Boussinesq and hydrostatic approximations, the three dimensional governing equations, including thermodynamics, become

$$(ub)_x + (wb)_z = 0 \tag{1}$$

$$(ub)_t + u(ub)_x + w(ub)_z = -(1/\rho_0)(Pb)_x + [K_M(ub)_z]_z + [A_M(ub)_x]_x \tag{2}$$

$$(eb)_t + u(eb)_x + w(eb)_z = [K_H(eb)_z]_z + [A_H(eb)_x]_x \tag{3}$$

$$\rho g = -P_z \tag{4}$$

$$\rho = \rho(T, S) \tag{5}$$

where x is horizontal axis to the east and z is positive upward with $z = 0$ at the mean free surface; b represents the channel width and is set to unity in our study; t is the time; ρ_0 is the reference density taken to be 1000 $\mathrm{kg\,m^{-3}}$, ρ is in-situ density, g the gravitational acceleration and P the pressure. e denotes either temperature T or salinity S. K_M and K_H, calculated with the turbulence closure model, are vertical eddy viscosity and diffusivities for momentum and thermodynamic variables (e) respectively; A_M and A_H are horizontal diffusivites, included to ensure numerical stability. They are taken to be the same and modeled by a simplified Smagorinsky formulation. The earth's rotation weakens the topographic control in general (Chao and Paluszkiewicz, 1991), but is excluded in this model since we are interested in a narrow channel, the width of which is always less than the internal Rossby radius. Bottom friction is included and is parameterized using a quadratic law in the model.

The numerical model uses a finite-difference method and solves the governing equations in the σ coordinate. It has a staggered C-grid and a leap-frog scheme

in time. It employs the mode-splitting scheme to compute the depth-integrated shallow water equations with a short time step and computes the internal mode with a larger time step. The Courant-Friedrichs-Levy (CFL) condition is used to limit the time steps and, in this model, becomes

$$\Delta t = \frac{\Delta x}{2C + U_{max}} \tag{6}$$

where Δx is horizontal grid spacing; C is either the external wave phase speed $(gH)^{1/2}$ or the fastest internal wave phase speed; and U_{max} is the maximum current velocity. U_{max} may be greater than C in some studies of interest to us and must be included.

The present model is a simplified version of the Blumberg and Mellor three dimensional ocean circulation model. More details concerning the original model can be found in Blumberg and Mellor (1987) and Mellor (1990).

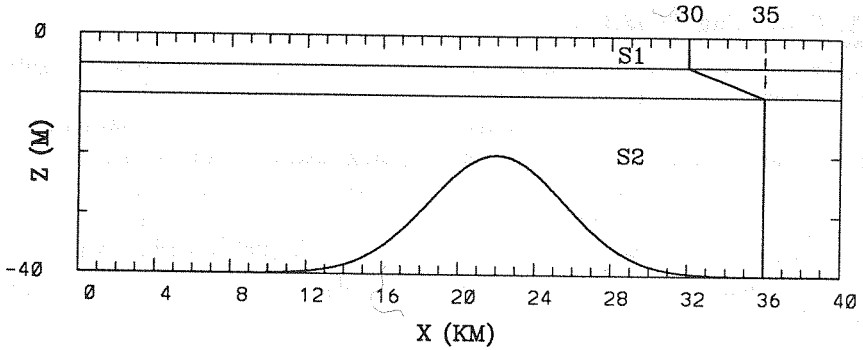

Figure 1. The model domain and coordinate system. A typical initial vertical stratification is also shown.

2.2. The Model Setup

We consider a channel 40 km long and 40 m deep with a sill (Figure 1). These dimensions are comparable to Manitounuk Sound in Hudson Bay (Gan and Ingram, 1992). The sill is centered at $x_0 = 22$ km with a Gaussian shape, $h_s = h_0 \exp(x - x_0)^2/R^2$. The h_0 is the height of the sill and R the characteristic half width, chosen to be 5 km. The ratio h_0/R determines the slope of the sill and is in the range of 3.2–4.8 $\times 10^{-3}$ for the cases to be studed. A constriction can also be introduced by solving equations (1) to (5) with a variable width b.

Considering the fact that in the coastal region, including sounds and inlets, the stratification is dominated by salinity, we assume a constant temperature $T = 10^{\circ}$C in the channel and solve only the salinity conservation equation for simplicity and without losing generality. The initial salinity structure is uniform along channel and the typical vertical distribution used in the model is also shown

in Figure 1. The density difference across halocline is approximately 4.0 kg m^{-3} The water column has a two-layer structure if being separated into two layers by $S = 32.5$ psu, a thin upper layer and a thicker lower one, which is typical in sounds and inlets and enables us to compare the model results with layer theory whenever appropriate. The number of σ levels were chosen so as to well resolve the halocline. The horizontal grid spacing is $\Delta x = 100$ m, which enables us to resolve the highly fluctuating solitary waves.

The sinsoidal barotropic tidal currents are forced at $x = 0$. We let the tidal period T_t be 12 hours for simplicity. The surface elevation and right-end barotropic velocity conditions are Orlanski type radiation. Although the model driving force is the barotropic tide, a baroclinic response can also arise because of many factors such as the stratification, flow interaction with topography and bottom friction. The baroclinic velocities are radiated at the boundaries at the estimated first mode internal wave speed. Advection conditions are used for salinity at both ends, which implies that incoming flow to the domain has a predetermined salinity and is not affected by the sill. To examine the effectiveness of the advection and radiation conditions, we doubled the domain length in a test calculation and found no significant differences in flow characteristics within the 40 km region.

3. RESULTS AND DISCUSSIONS

Table 1 gives a list of cases studied. All calculations start with a zero current condition and statistically stable dynamic states are achieved in about 2.0 days. Analyses are based upon the results after 3 days. We assume hereafter that flooding represents the flow from left to right and ebbing from right to left. Since the wave length of the barotropic semi-diurnal tides is much longer than the length of the channel of 40 km and the external Froude number is always much less than unity ($F_{e(max)} < 0.1$) in this study, the external response has little contribution to the internal hydraulics and will not be discussed.

Table 1. The studied cases.

Case	Sill (h_0/H)	ΔS (psu)	h_0 (m)	U_m (m s^{-1})	Δx (m)	σ Levels
1	0.4	5.0	16.0	0.3	100	27
2	0.5	5.0	20.0	0.1	100	27
3	0.5	5.0	20.0	0.3	100	27
4	0.5	15.0	20.0	0.3	100	27
5	0.6	5.0	24.0	0.3	100	27

For the convenience of analysis, we will use a two-layer approach when appropriate. We separate the water column into two layers by the isohaline $S = 32.5$ psu. The vertical averaged velocities in each layer are thus comparable to the two layer theory counterparts. Froude numbers can be defined for each layer, respectively, as $F_i^2 = u_i/(g'H_i)$, where H_i is layer depth and $i = 1, 2$, and the composite Froude number as $G^2 = F_1^2 + F_2^2$.

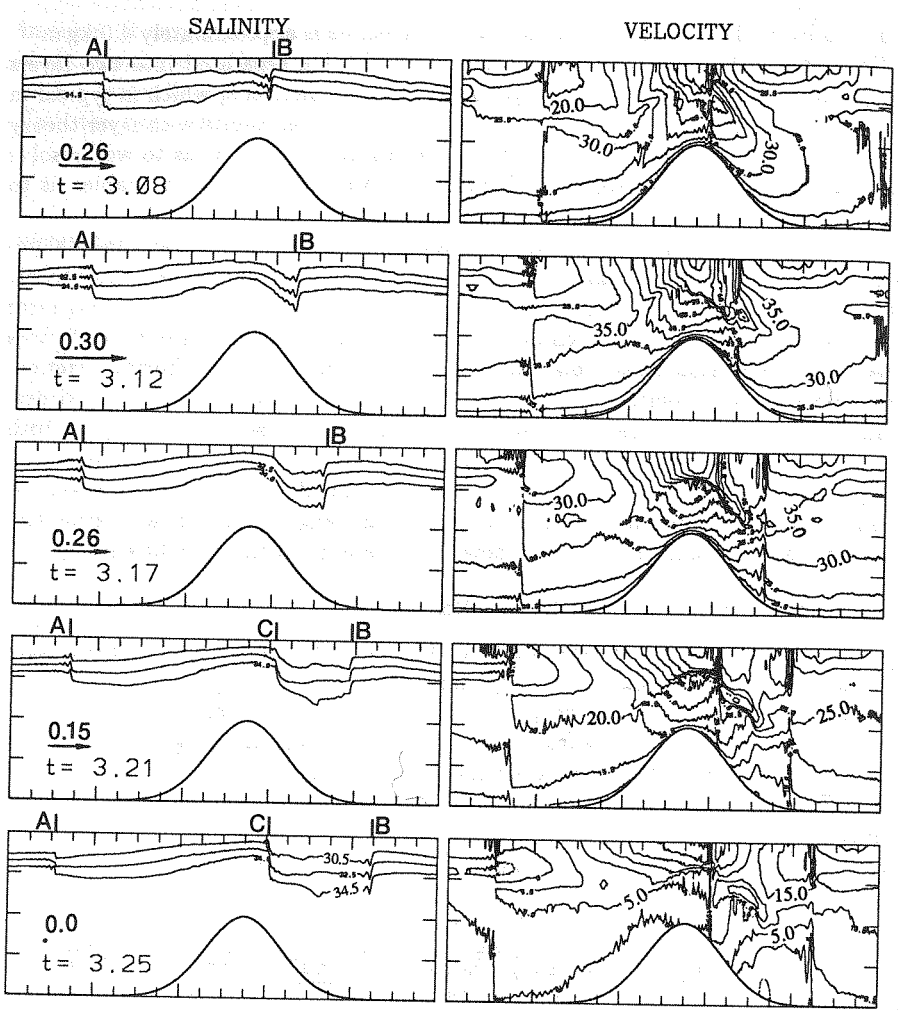

Figure 2. The salinity and horizontal velocity contours and their variations with varing tidal flows, plotted at an interval of an hour. Contour intervals are 2.0 psu and 5.0 cm s^{-1}, respectively. The arrows indicate the forced tidal current at $x = 0$. Labels (A, B, C and D) track the internal wave propagation.

3.1. The General Flow Features.

We first describe the flow field under the forcing of semi-diurnal tides as in Case 3 of Table 1. Figure 2 shows the isohaline displacements and the horizontal velocity distribution in flood stage at a time interval of 1 hour. The forced tidal currents at the left boundary are also shown with each frame. Note there is a slight delay of flow response in the channel. At the flooding stage, the current increases in the lower layer first. At $t = 3.12$ days, the tidal flow reaches maximum at the left boundary. Upstream of the sill, the flow is nearly uniform vertically but near the sill crest a two-layer structure formed, with high velocity near the surface and lower velocity below. The flow is forced to grow at the upstream side and thus moves the isohalines upward and increases the vertical gradient, as seen in Figure 2. The local maximum velocity occurs at $t = 3.17$ days and the horizontal velocity gradient increases at $x = 24$ km. One hour later, the gradient reaches maximum ($\partial u/\partial x \approx 5\times10^{-4}$) and an internal jump occurs. Corresponding to such a velocity field, the isohaline displacements change drastically and can drop more than 5 m within 0.5 km in the horizontal, as an indication of the jump (The jump will be discussed in more detail shortly). The isohaline slope at the jump steepens as the flow weakens. The internal bore thus formed moves upstream when tidal currents reverse at $t = 3.25$ and evolves into solitons. The formation of solitons from a large amplitude bore is due to nonlinearity and has been successfully explained by the KdV equation (i.e. Smyth and Holloway, 1988). However, the solitons here appear to have relatively smaller amplitudes. An explanation may be that the hydrostatic approximation suppresses their growth. Because the solitons have a horizontal scale of hundreds meters and are highly fluctuating, a non-hydrostatic model would be an improvement.

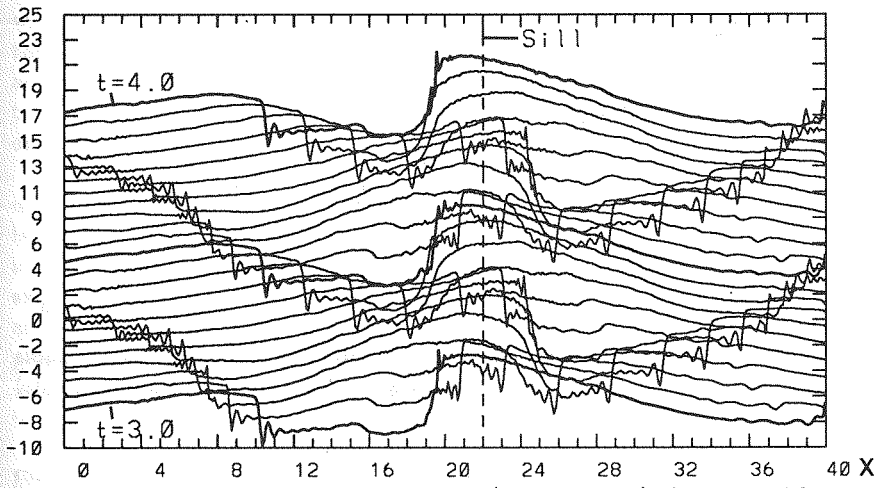

Figure 3. The evolution of the isohaline ($S = 32.5$ psu) elevation within two tidal cycles for Case 3. Each subsequent line is offset one meter.

Figure 3 shows the evolution of isohaline $S = 32.5$ psu, with each subsequent curve offset by 1 m. The internal wave propagation can be seen. The waves are formed at the leeside of the sill and propagate across and then away from the sill in two branches. The left branch originated at $x = 25$ km during the flood (left to right flow) but propagated to the left when the tide slackens. The right branch formed at $x = 19$ km during the ebb and propagated to the right when the flow reverses. The internal bore/soliton propagation has the characteristics of the first-mode internal wave, and can be expressed as (Hibiya, 1988):

$$dx/dt = U(x,t) + c_1(x) \tag{7}$$

where $U(x,t)$ is the tidal advection velocity and can be evaluated by averaging the velocity vertically over the isohalines. The c_1 is estimated by a two layer approximation for limited water depth, $c_1^2 = g'H_1H_2/H$, where H_1 and H_2 are upper and lower water depths, respectively, and $H = H_1 + H_2$. If the sill height $h_0 = 20$ m, c_1 ranges from 0.44 at the crest to 0.50 m s^{-1} in the flat regions. The wave crest paths against time are plotted in Figure 4. We track the waves labeled as A, B, C and D in Figure 2 and also plot them in Figure 4. They agree very well. In this case, the current can be comparable and even larger (or supercritical) than the wave speed and, therefore, the paths are curves though the c_1 varies in a small range because of the modification of varing tidal current $U(x,t)$. The second and higher modes can not be identified from the model results, likely due to the hydrostatic approximation and the near two-layer density structure.

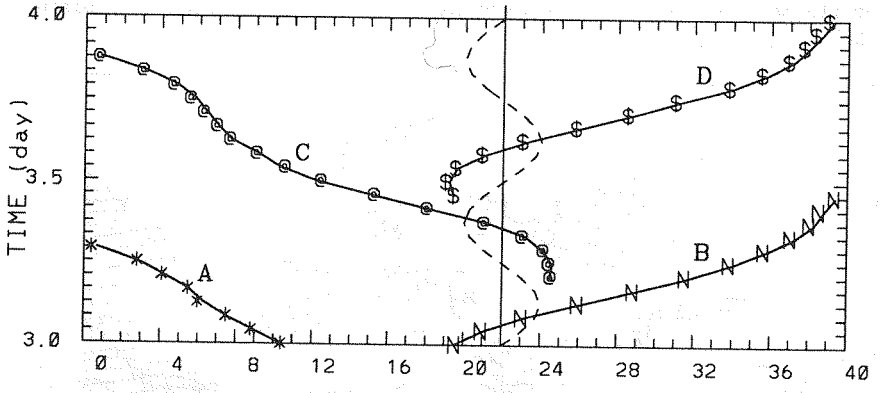

Figure 4. The characteristics for the first mode internal wave. The symbols are obtained by tracking wave crests like in Figure 2. Dashed line shows the tidal flow applied at the $x = 0$.

If we reduce the strength of the tidal flow (Case 2) so that the maximum composite Froude number is less than one throughout the tidal cycle, internal waves are generated near the sill center and the wave crest paths are nearly

straight because of the minor modification by advective currents. This case can thus be considered the weak advection case of Hibiya (1986). Comparing Case 2 and Case 3, we find that the origins of the internal bores shift to the downstream sides of the sill. The displacement of the isohaline in Case 3 is much larger, not being proportional to the increase of forcing, than that in the weak forcing case.

3.2. The Internal Hydraulic Jump.

Following layer theory, the flow is called supercritical if the composite Froude number $G^2 > 1$, and subcritical if $G^2 < 1$. The locations where $G^2 = 1$ are the critical points.

When the flow is subcritical the interfacial layer moves upward near the sill and remains symmetrical about the sill center. The interface deflection causes the upper layer compression and increases upper layer velocities. Because of the thinner thickness, the upper layer is more active than lower layer in view of the higher F_1 than F_2 and G^2 is controlled by F_1^2. The crest point reaches a critical condition first and then becomes supercritical when the flow becomes stronger. There are two critical points, one at the upstream and the other at the downstream of the sill. Figure 5 gives the variation of composite Froude number along the channel and its evolution in time, each subsequent G^2 curve being displaced one unit upward. It can be seen that the Froude number along the channel is nearly symmetrical with the sill center at early stage. For peak tidal currents ($3.12 < t < 3.21$), the downstream critical point is nearly stationary at $x = 25$ km and there is a sudden drop of G^2 from supercritical to subcritical, which represents a discontinuity of the velocity field, or a large horizontal velocity change over a narrow region. The isohalines plunge at the critical location during the same period. The Froude number features can be understood easily in conjuntion with the salinity and horizontal velocity structure, as shown in Figure 2. Noticing the high shears and the high velocity water patch in the middle of water column at the lower interfacial layer, the vertical structure of velocity has similar features to that observed in Observatory Inlet by Farmer and Denton (1985) when a jump occured.

Because we have an active upper layer, the jump, causing a thickening of the upper layer, dissipates upper layer kinetic energy to lower layer. If the lower layer is active there will be an uplift of the interface and the energy transfer is upward. An interesting and complicated process, in which the active layer switches from upper to lower layer, may occur if one properly chooses the forcing and the stratification. At the upper layer critical point of $F_1^2 = 1$, the interface plunges, and therefore reduces the lower layer thickness and may increase the velocity as well. Hence, the lower layer becomes active and causes the interface to jump upward immediately after the plunge.

An increase of sill height will generate higher velocities in the sill region and a longer supercritical area. The flow becomes more energetic, not only because of an increase of the velocity, but also due to the stronger interaction with stratification.

While the basic processes are same, different sill heights result in different jump locations (Figure 6). The higher the sill, the further the jump is located away from the sill center. A 4 m increase of sill height shifts the jump location about 2 km downstream, which is due to the stronger advection induced over the topography. In addition to changes in location, the jumps also show larger drops for higher sills, which indicates more severe jumps. Both the amplitude and formation site of the internal bores are affected.

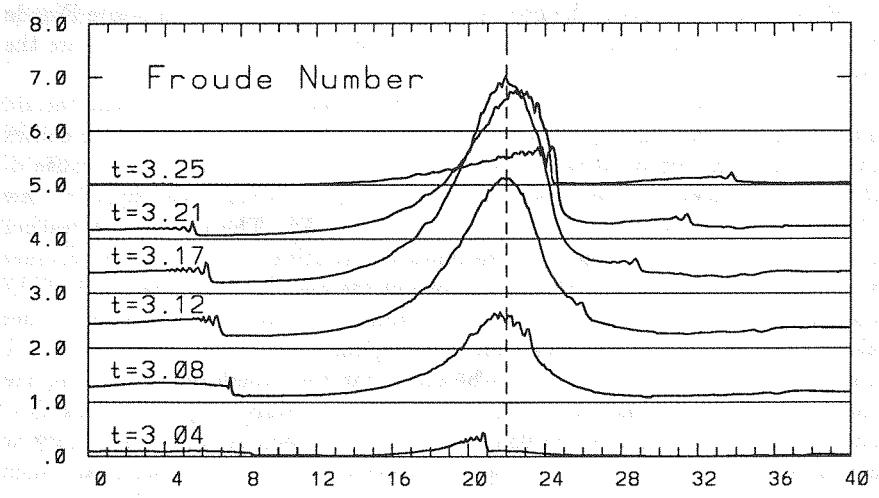

Figure 5. Composite Froude numbers G^2, plotted along channel and with time. Each subsequent curve is offset one unit upward.

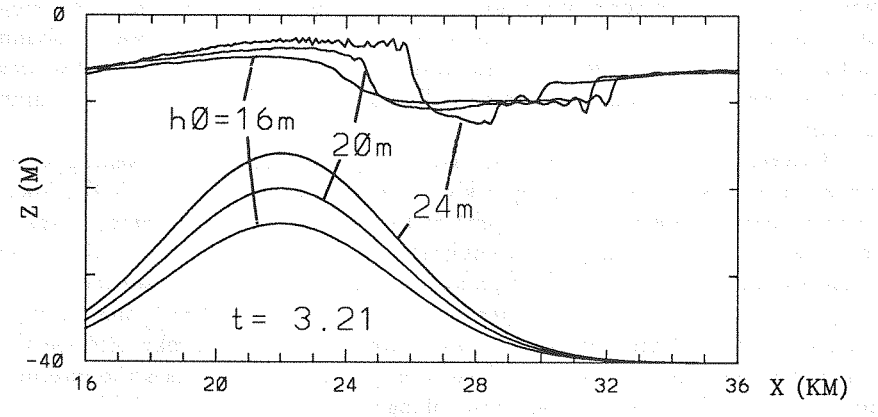

Figure 6. Comparison of isohaline elevations ($S = 32.5$ psu) corresponding to three different sill heights, $h_0 = 16$, 20, 24 meters (cases 1, 3 and 5) respectively.

3.3. The Vertical Mixing Associated With Jump.

Earlier studies (i.e. Lewis, 1985) indicated that intense mixing events were either initiated or coincided with the existence of critical or subcritical flow. When G^2 is only just supercritical (a weak jump), some of the energy can be radiated away in the form of internal waves, but for higher G^2 insufficient energy can be dissipated in the waves alone and they must break. The high kinetic energy upstream of the critical point needs to match the low kinetic energy regime downstream. A jump occurs to partly convert kinetic energy into potential energy through vertical mixing. As a consequence of the mixing, the vertical gradient of salinity is reduced as shown in Figure 8*b* (isohalines are further apart than before).

Strong mixing occurs within each homogeous layer but does not change the water properties in each of the layers. Our interest is the mixing between the upper layer low salinity water and the lower layer high salinity water. Figure 7*a* shows the turbulence eddy viscosity, K_M, at the layer interface and the vertical velocity contours for Case 3. At this time during the flood, the critical or transition point from supercritical to subcritical is at $x = 25$ km and a jump occurs. Immediately downstream of the jump there is high turbulent kinetic energy and strong oscillating vertical motions. Note that away from jump region, K_M is so low that it can not be distingushed from the horizontal axis in the plot. Accompanying the high K_M, strong vertical motions take place, with values reading 0.2–0.3 cm s^{-1} (Figure 7*b*).

Figures 7*c*, *d* give the Richardson number and salinity in an enlarged region for $t = 3.21$ days. The gradient Richardson number is defined as $R_i = -\frac{g}{\rho}\frac{\partial\rho/\partial z}{(\partial u/\partial z)^2}$, and the values below 20 and the corresponding salinity in the range of 30.2 to 34.8 are plotted. The '+' indicates the points of instabilities where $R_i < 0.25$. The unstable points are found upstream of the jump that occurs at $x = 25$ km. The velocity shear ($\partial u/\partial z$) reaches a maximum value in the region and is believed to be responsible for the instability (see Figure 2). This is consistent with other results (i.e. Wood and Simpson, 1984). From his experimental results, Lawrence (1985) indicated that the primary cause of mixing in flows with an internal hydraulic jump is not the jump itself, but a shear layer upstream of the jump. However, the instability also occurs in the downstream neigborhood of the jump. The unstable points at $x \approx 29$ km are likely caused by both velocity shear and a lower density gradient.

It is interesting to note two phenomena in our results. The first, vertical motions appear to occur more often with the solitons. After K_M decreases to insignificance the vertical velocities are still strong, and even slightly gain in intensity when associated with the solitons away from the sill. The dissipation of solitons associated with the internal waves provides energy for vertical mixing, similar to that found by Sandstrom and Elliott (1984). The lower strength of vertical velocities at the jump is probably due to the bottom slope that tends to suppress vertical motion. The strongest vertical motions do occur at the jump

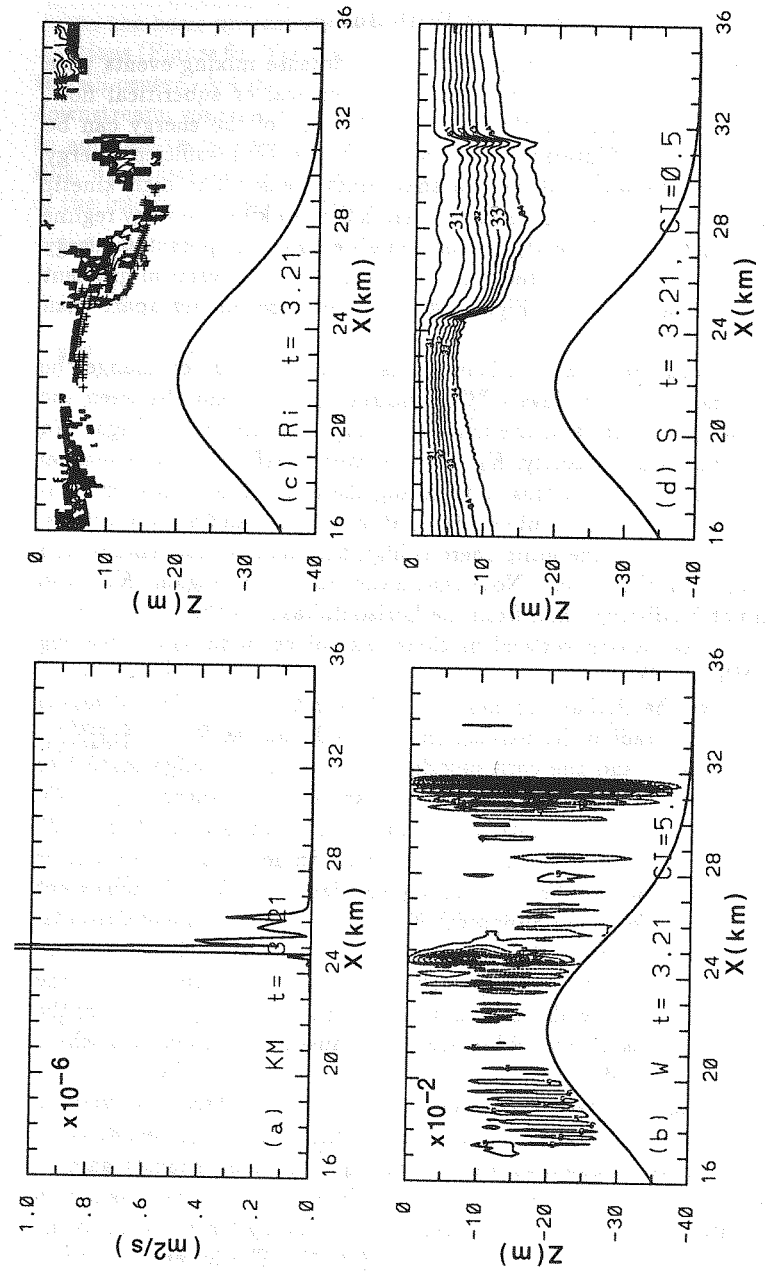

Figure 7. (a) Turbulent kinetic energy along the isohaline $S = 32.5$ psu. (b) Vertical velocity contours (unit: cm/s). Dashed lines are negative and the zero lines are not shown. (c) The distribution of low Richardson number points within the halines. The '+' represents the points of $R_i \leq 0.25$. (d) Salinity contours.

in the case of a constriction with a flat bottom (not shown). The second point of interest is that the mixing at the flood stage interacts with that from previous ebb. In Figure 7*d*, the soliton '*A*', generated in previous ebb stage, is propagating to the right while a new jump is forming at '*B*' with its downstream mixing. The mixing due to '*A*' and that due to '*B*' overlap in the region '*C*' and thus gives a minimum salinity gradient in the vertical. This region will expand when '*A*' and '*B*' travel further apart (in opposite directions).

The echo sounder images obtained in Observatory Inlet by Farmer and Denton (1985) showed turbulent flow at the jump and further downstream. Ingram et al. (1989) and Gan and Ingram (1992) observed saltier water in the upper layer between two mooring stations in Manitounuk Sound. They concluded that solitary waves and the following bores were responsible for the vertical mixing. That solitary waves and bores enhance mixing is also suggested by our model results.

4. SUMMARY AND CONCLUSION

We have developed an x–z plane, primitive equation hydraulics model with a turbulent closure scheme and applied the model in studying the internal waves, hydraulic jumps and associated mixing for the interaction of tidal flow and a bottom sill in stratified water.

For certain combinations of sill height and tidal flow the flow over the sill will be supercritical. Downstream of the sill, a jump occurs at the critical location of transition from supercritical to subcritical. A large amplitude internal bore is formed and propagates across the sill crest when tide slackens, and then evolves into solitons because of nonlinearity. The bore/soliton propagation has the characteristics of first-mode internal waves. Instabilities occurs both upstream and downstream of the jump, mainly due to the high velocity shears. The most effective mixing occurs at the downstream of the jump. The mixing process is maintained along the traveling soliton. Increased sill height increases the nonlinearity of the flow and results in a more prominent jump that is displaced downstream. If the halocline is lowered downward closer to sill, the lower layer water becomes more active and plays a role in generating the jump.

Time dependence is important in this study, not only because we have studied internal wave propagation, but also because the jump is formed gradually. In the cases examined, there are always solitary waves travelling over the sill region and they will interact with the forthcoming jump. This implies that the flow condition is not in steady state, at least for our forcing and geometry. The hydrostatic approximation is appropriate to describe the internal hydraulic jump and the large amplitude bore in our experiments. However, it seems to have resulted in smaller soliton amplitudes than observed.

ACKNOWLEDGMENTS

The authors thank Drs. Lie-Yauw Oey and Joel Wesson for helpful discus-

sions. The financial support of NSERC, NCE, Fonds FCAR and GIROQ are gratefully acknowledged.

APPENDIX. REFERENCES

Armi, L. and D.M. Farmer, 1986: Maximal two-layer exchange through a contraction with barotropic net flow. *J. Fluid Mech.*, 164, 27–51.

Blumberg, A.F. and G.L. Mellor, 1987: A description of a three-dimensional coastal ocean circulation model. In *Three Dimensional Ocean Models*, Amer. Goephys. Union, Washington, DC, 1–16.

Chao, S-Y. and T. Paluszkiewicz, 1991: The hydraulics of density currents over estuarine sills. *J. Geophys. Res.*, 96, 7065–7076.

Farmer, D.M. and R.A. Denton, 1985: Hydraulic control of flow over the sill in Observatory Inlet. *J. Geophys. Res.*, 90, 9051–9068.

Farmer, D.M. and J.D. Smith, 1980: Tidal interaction of stratified flow with a sill in Knight Inlet. *Deep Sea Res.*, 27A, 239–254.

Gan, J. and R.G. Ingram, 1992: Internal hydraulics, solitons and associated mixing in a stratified sound. *J. Geophys. Res.*, 97, 9669–9688.

Geyer, W.R., 1990: Time-dependent, two layer flow over a sill. In *The Physical Oceanography of Sea Straits*, edited by L.J. Pratt. 421–432. Kluwer, Boston.

Hibiya, T., 1986: Generation mechanism of internal waves by tidal flow over a sill. *J. Geophys. Res.*, 91, 7697–7708.

Hibiya, T., 1988: The generation of internal waves by tidal flow over Stellwagen Bank. *J. Geophys. Res.*, 93, 533–542.

Ingram, R.G., J.C. Osler and L. Legendre, 1989: Influence of internal wave induced vertical mixing on ice algal production in a highly stratified sound. *Estuarine Coastal Shelf Sci.*, 29, 435–446.

Lawrance, G.A., 1985: The hydraulics and mixing of two-layer flow over an obstacle. Rep. No. UCB/HEL-85/02, UC, Berkeley, California.

Lewis, R.E., 1985: Intense mixing periods in an estuary. In *Turbulence and Diffusion in Stable Environ.*, edited by J.C.R. Hunt. 319pp, Oxford, New York.

Matsuura, T. and T. Hibiya, 1990: An experimental and numerical study of the internal wave generation by tide-topography interaction. *J. Phys. Oceanogr.*, 20, 506-521.

Mellor, G.L., 1990: User's Guide for A Three-Dimensional, Primitive Equation, Numerical Ocean Model. *Tech. Rep.*, Atmos. and Oceanic Sci. Prog., Princeton Univ., Princeton, NJ.

Sandstrom, H. and J. Elliott, 1984: Internal tide and solitons on the Scotian Shelf: a nutrient pump at work. *J. Geophys. Res.*, 89,6415–6426.

Smyth, N.F. and P.E. Holloway, 1988: Hydraulic jump and undular bore formation on a shelf break. *J. Phys. Oceanogr.*, 18, 947–962.

Wood, I.R. and J.E. Simpson, 1984: Jumps in layered miscible fluids. *J. Fluid Mech.*, 140, 329–342.